Supporting information

Controllable fabrication of stimuli-responsive fluorescent silica nanoparticles with a tetraphenylethene-functionalized carboxylate gemini surfactant

Saisai Yan,[ab] Zhinong Gao,*[ab] Jia Han,[ab] Zhengqin Zhang,[ab] Fei Niu[a] and Yingfang Zhang[ab]

[a] Key Laboratory of Biomedical Polymers of Ministry of Education, College of Chemistry and Molecular Sciences, Wuhan University, Wuhan 430072, Hubei, P.R. China.

[b] Engineering Research Center of Organosilicon Compounds & Materials of Ministry of Education, College of Chemistry and Molecular Sciences, Wuhan University, Wuhan 430072, Hubei, P.R. China.

*Corresponding author: Zhinong Gao

E-mail: gzn@whu.edu.cn

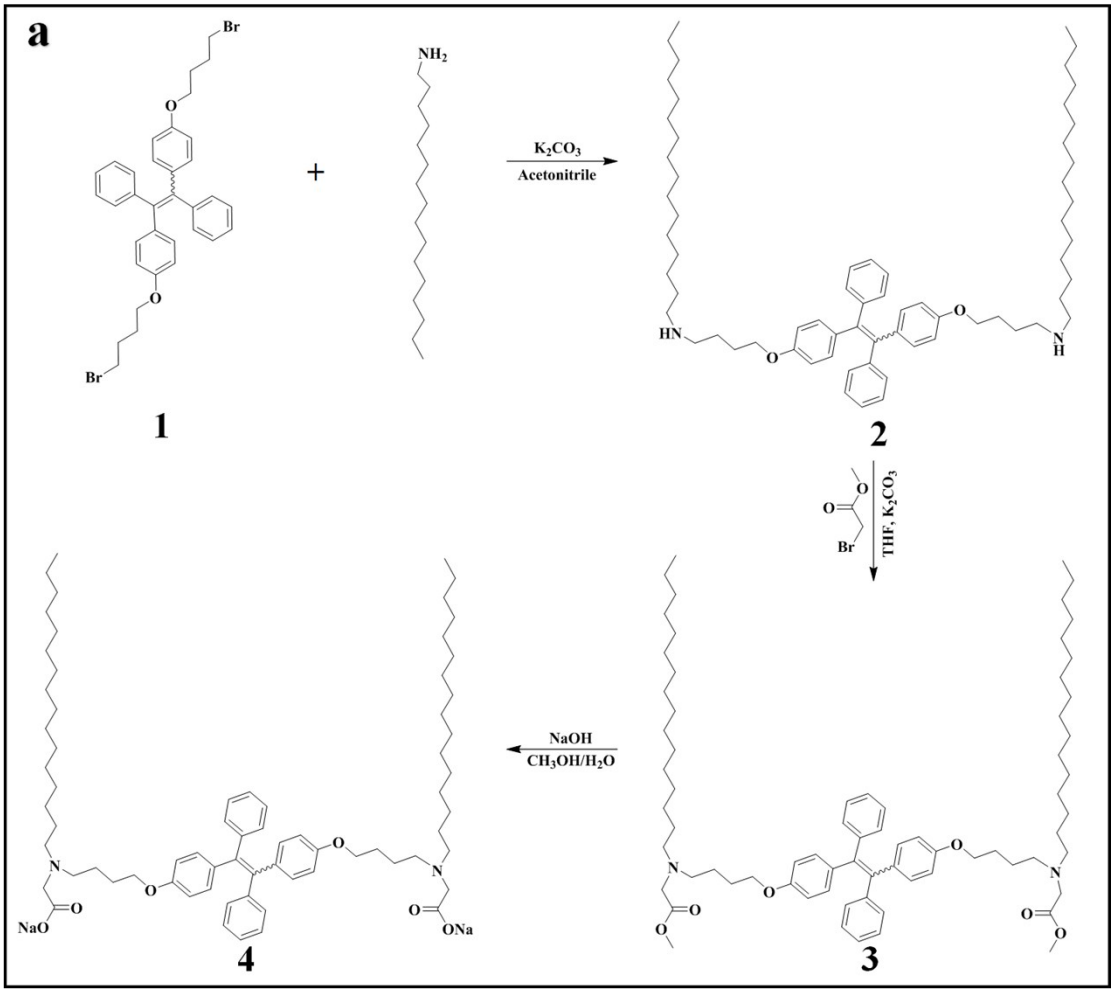
a
Br
NH2
K2CO3
Acetonitrile
1
2
THF, K2CO3
3
NaOH
CH3OH/H2O
4
NaO
ONa
HN
NH

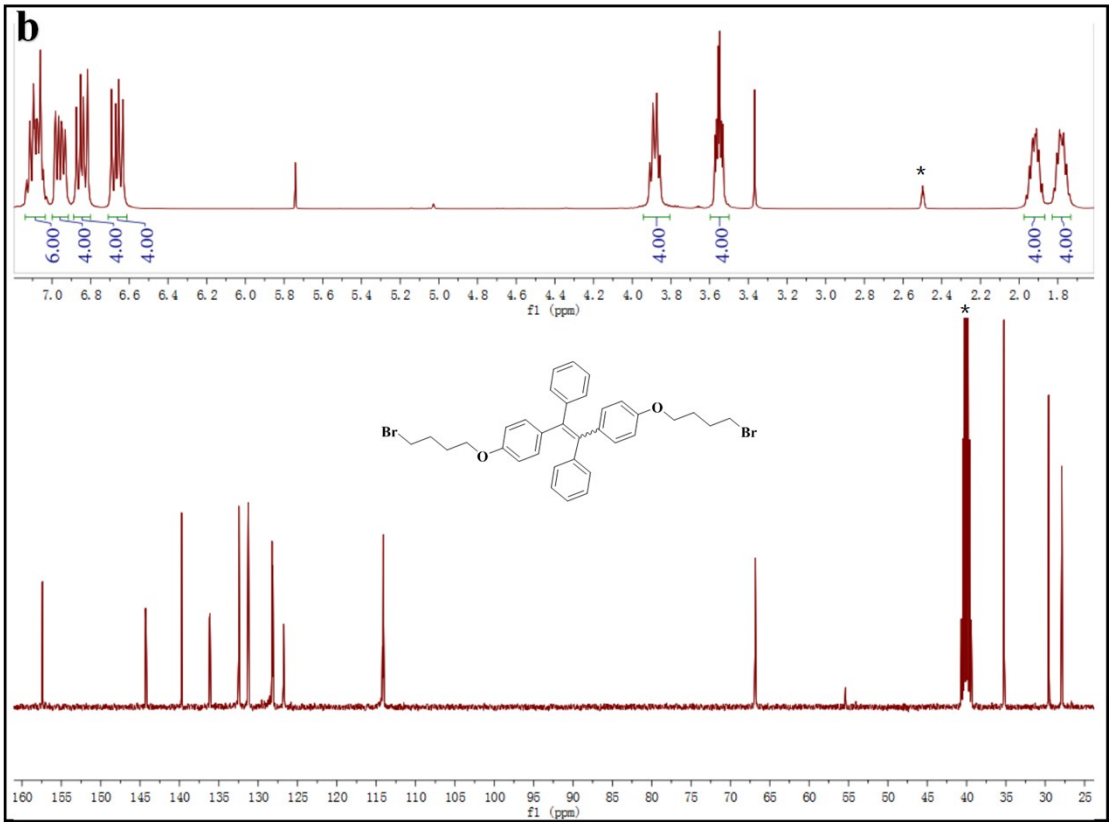
b
6.00
4.00
4.00
4.00
4.00
4.00
4.00
4.00
f1 (ppm)
Br
Br
f1 (ppm)

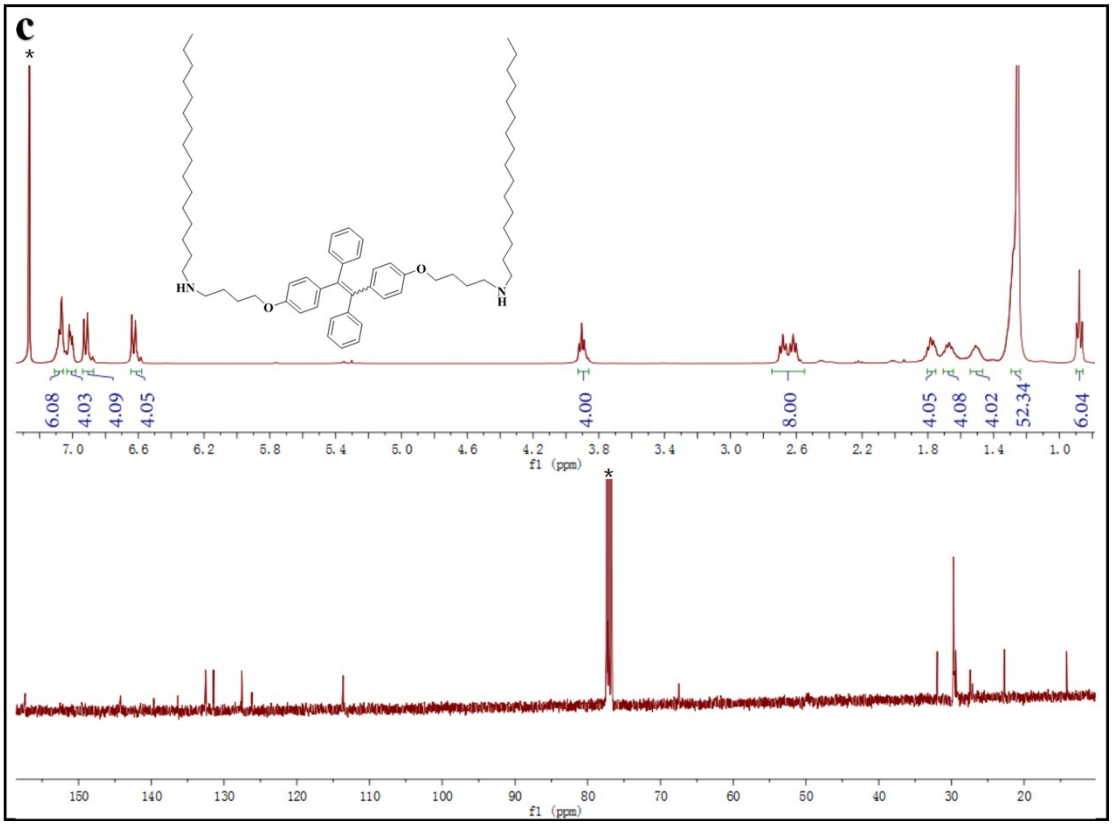
c
*
HN
O
O
N
H
6.08
4.03
4.09
4.05
4.00
8.00
4.05
4.08
4.02
52.34
6.04
7.0 6.6 6.2 5.8 5.4 5.0 4.6 4.2 3.8 3.4 3.0 2.6 2.2 1.8 1.4 1.0
f1 (ppm)
*
150 140 130 120 110 100 90 80 70 60 50 40 30 20
f1 (ppm)

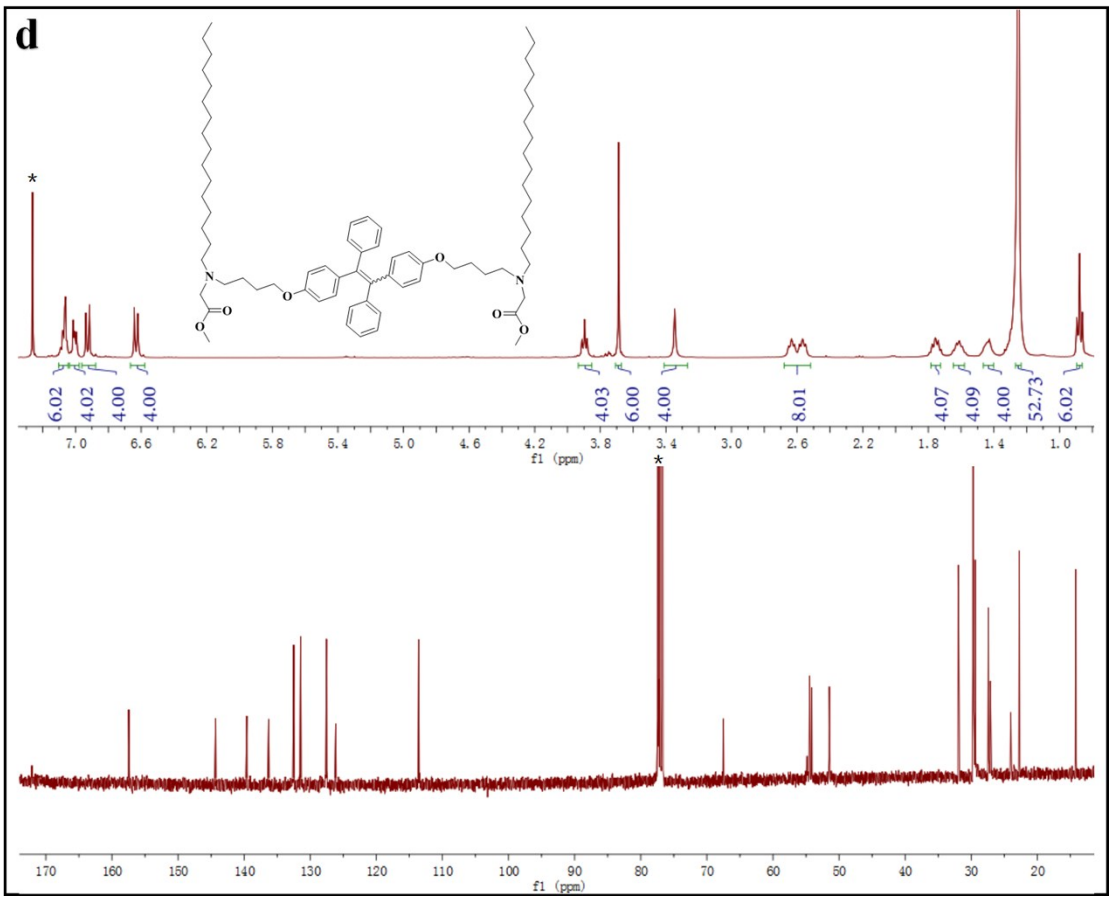
d
*
N
O
O
O
O
O
N
O
O
6.02
4.02
4.00
4.00
4.03
6.00
4.00
8.01
4.07
4.09
4.00
52.73
6.02
7.0 6.6 6.2 5.8 5.4 5.0 4.6 4.2 3.8 3.4 3.0 2.6 2.2 1.8 1.4 1.0
f1 (ppm)
*
170 160 150 140 130 120 110 100 90 80 70 60 50 40 30 20
f1 (ppm)

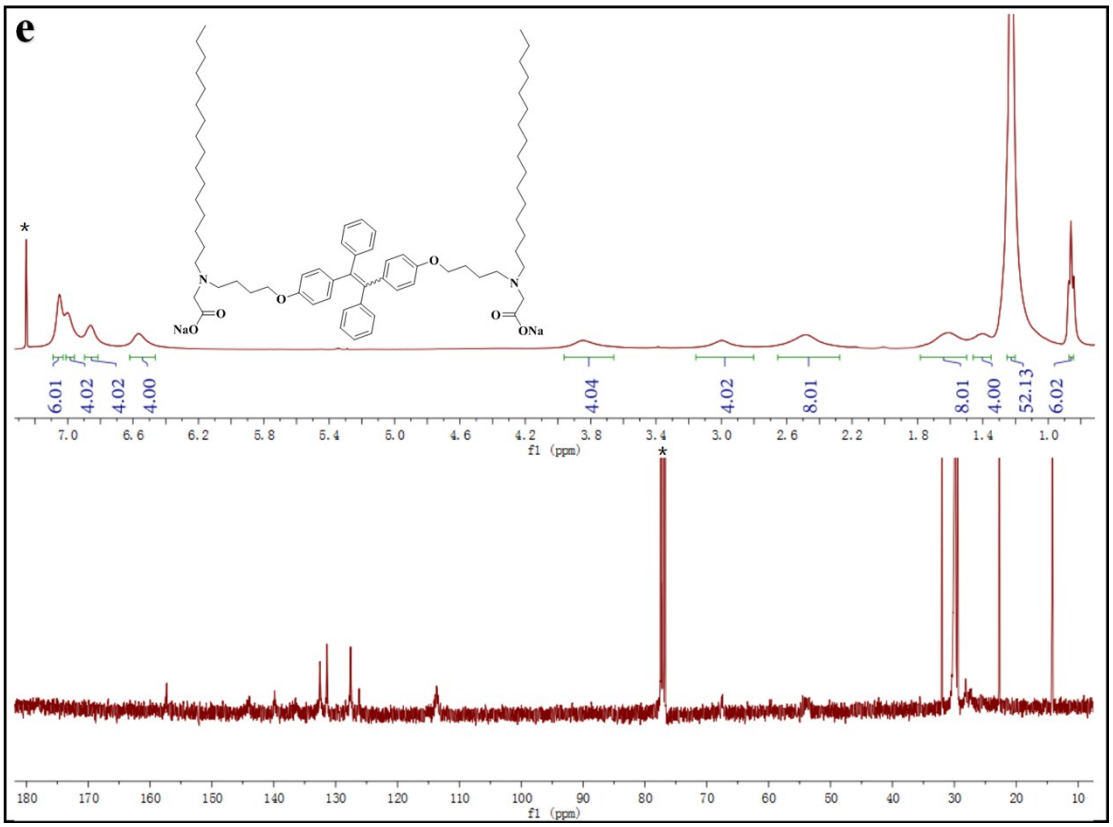

Scheme S1. (a) Synthetic route of the TPE-functionalized carboxylate gemini surfactant N_{16}-TPE-N_{16} (**4**). The corresponding ^{1}H and ^{13}C NMR spectra of compound **1** (b), **2** (c), **3** (d) and **4** (e).

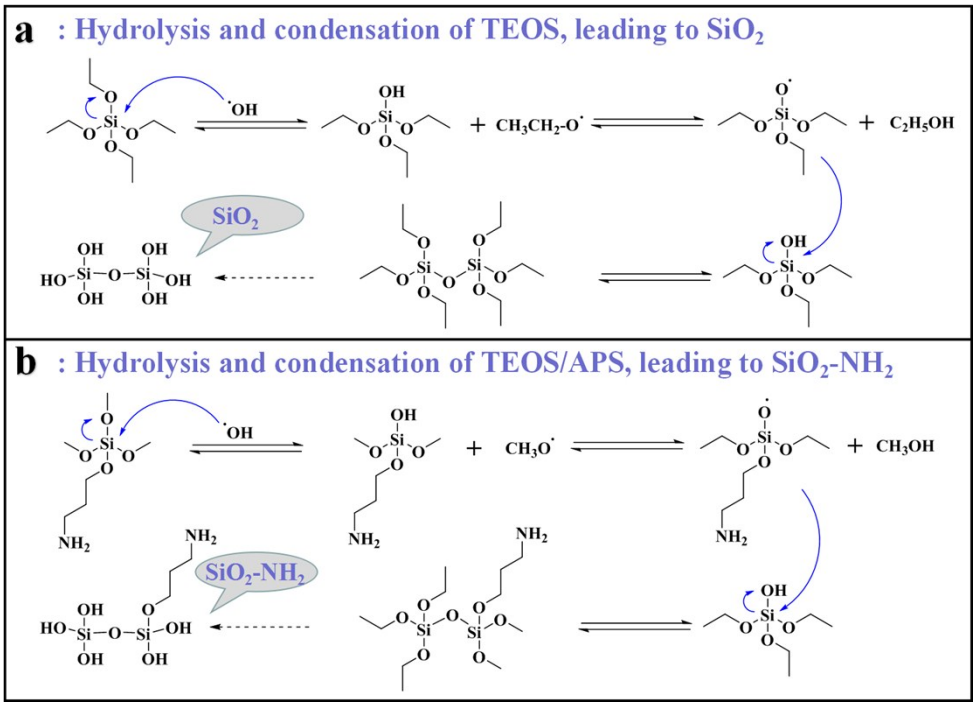

Scheme S2. Hydrolysis and condensation reactions of silane precursor TEOS for SiO_2 (a) and mixed organosilane precursors TEOS/APS for SiO_2-NH_2 (b).

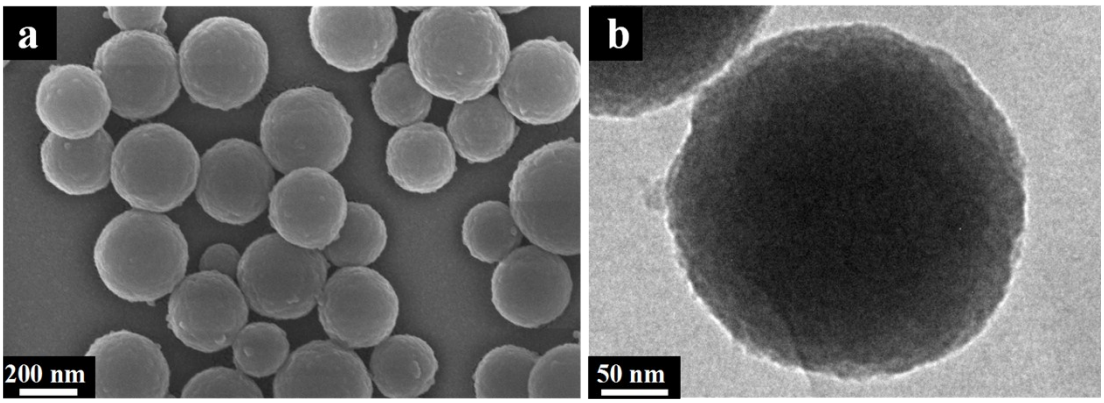

Figure S1. Representative SEM (a) and TEM (b) images of SiO_2-NH_2.

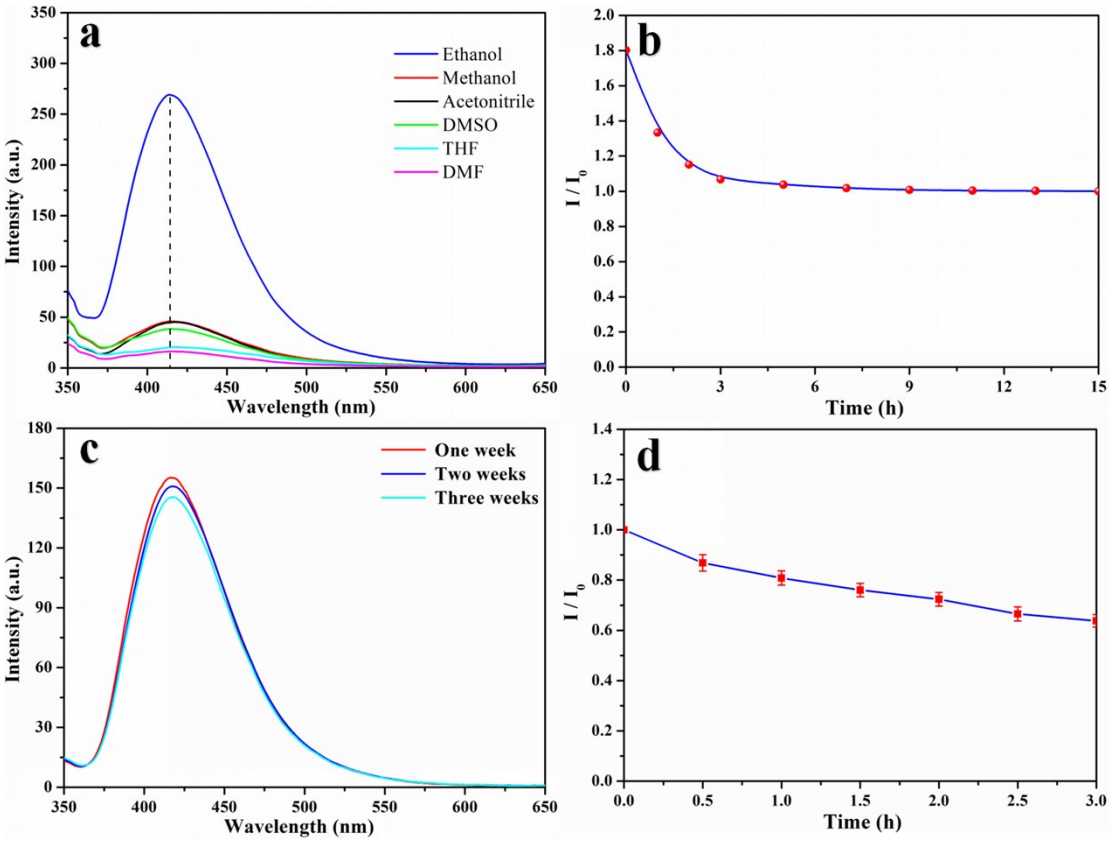

Figure S2. (a) Fluorescence spectra of SiO_2-NH_2-F induced by other water-soluble organic solvent (0.4 mg/mL). (b) Fluorescence intensity ratios of SiO_2-NH_2-F in aqueous dispersion (0.4 mg/mL), I_0 is the final fluorescence intensity at 416 nm and I is the corresponding fluorescence intensity at different times. (c) Time-dependent evolution of the fluorescence intensity of SiO_2-NH_2-F. (d) Photostability of SiO_2-NH_2-F upon continuous UV excitation. I_0 is the initial fluorescence intensity at 416 nm and I is the fluorescence intensity of the samples after UV irradiation.

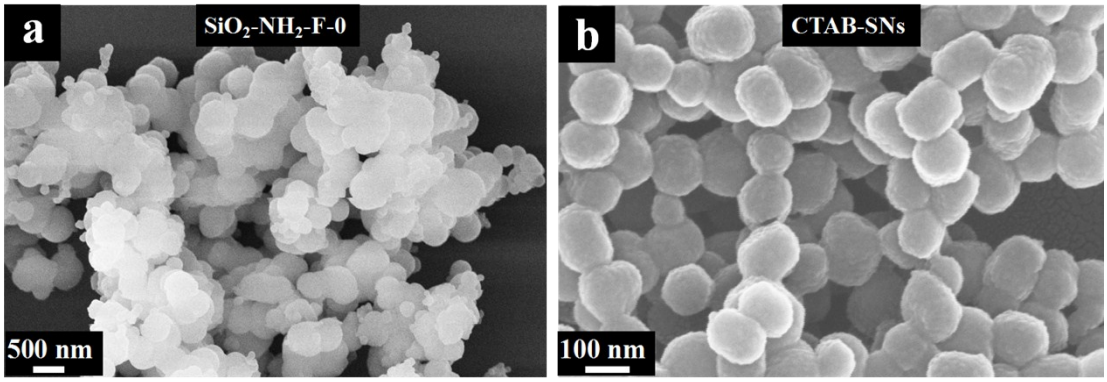

Figure S3. Representative SEM images of SiO_2-NH_2-F-0 (a) and CTAB-SNs (b).

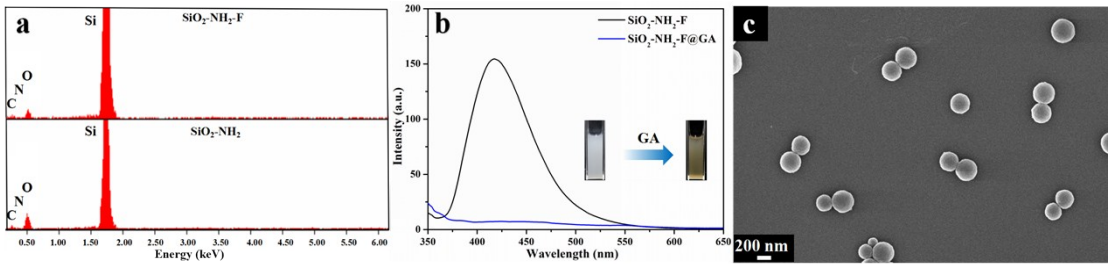

Figure S4. (a) EDX patterns of SiO_2-NH_2 and SiO_2-NH_2-F. (b) Fluorescence spectra of SiO_2-NH_2-F and SiO_2-NH_2-F@GA. Inset: Photographs of SiO_2-NH_2-F and SiO_2-NH_2-F@GA taken under the room light. (c) SEM images of SiO_2-NH_2-F@GA.

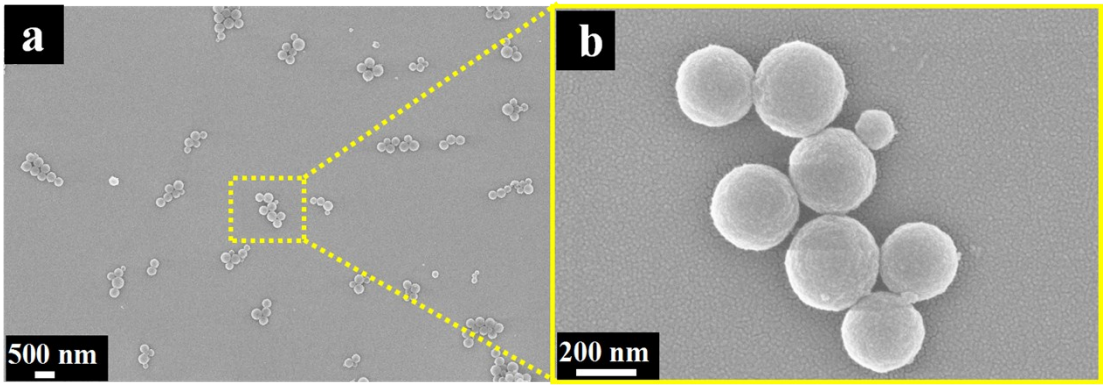

Figure S5. SEM images of SiO_2-NH_2-F in the dry powder.

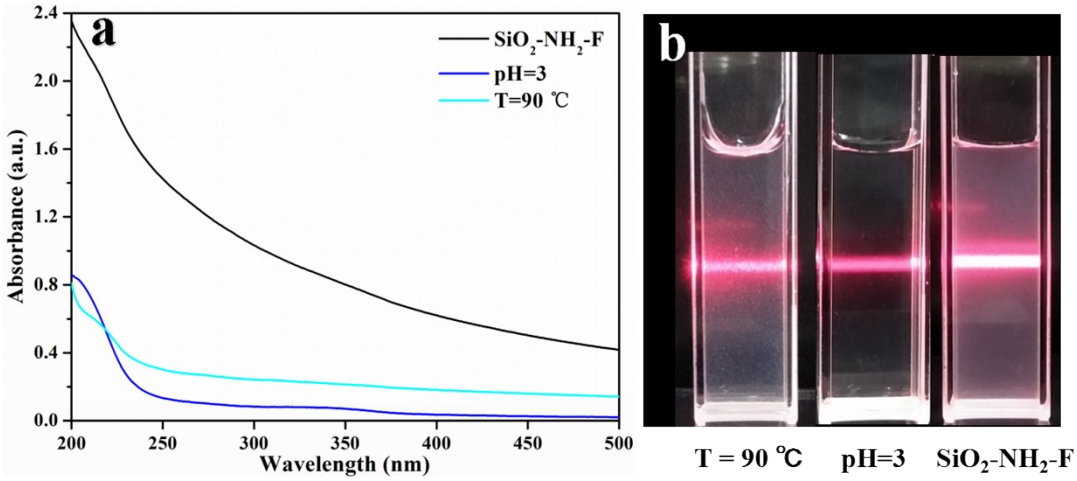

Figure S6. (a) Absorption spectra of SiO_2-NH_2-F at different states. (b) Tyndall phenomenon of SiO_2-NH_2-F aqueous dispersion at different states.

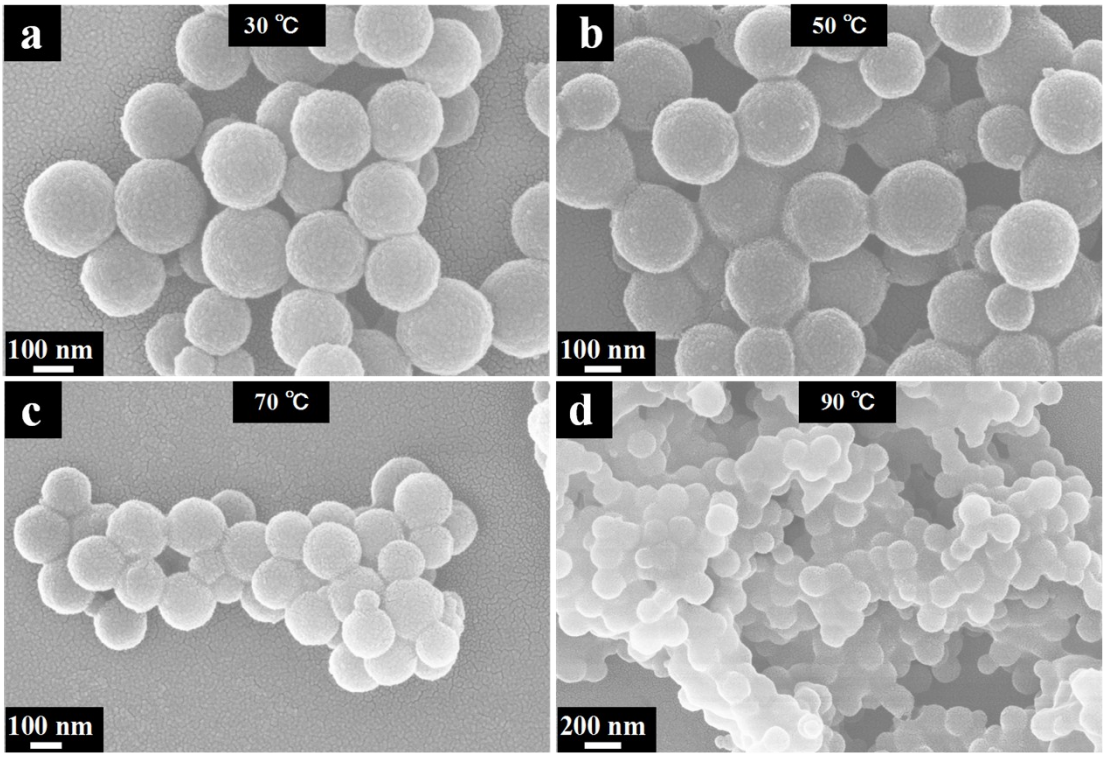

Figure S7. SEM images of SiO_2-NH_2-F treated with different temperatures: (a) 30, (b) 50, (c) 70, (d) 90 ℃.

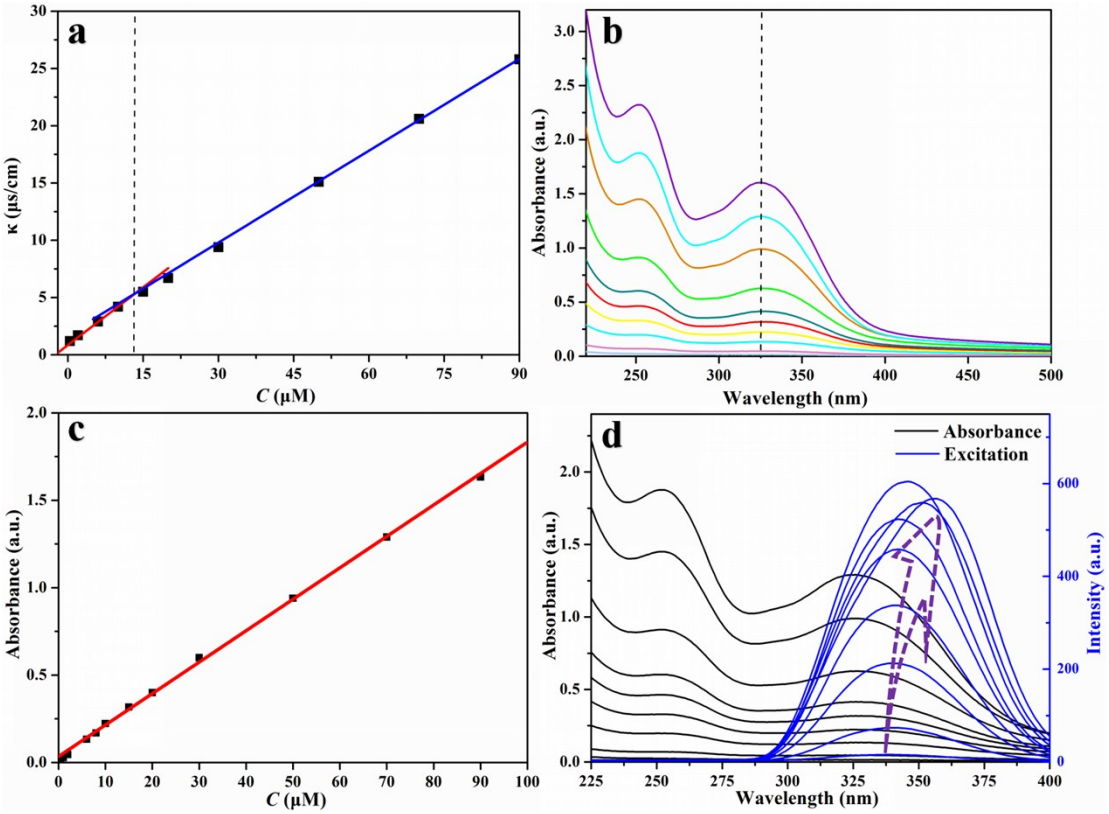

Figure S8. (a) Plot of conductivity (κ) versus the concentration of N_{16}-TPE-N_{16}. (b) Absorption spectra of N_{16}-TPE-N_{16} at different concentrations. (c) The linear relationship between the concentrations of N_{16}-TPE-N_{16} and absorbance data at 325 nm by the UV-Vis analysis. (d) UV-Vis absorption (black line) and fluorescence excitation (blue line) spectra of N_{16}-TPE-N_{16} recorded below and above the CMC.

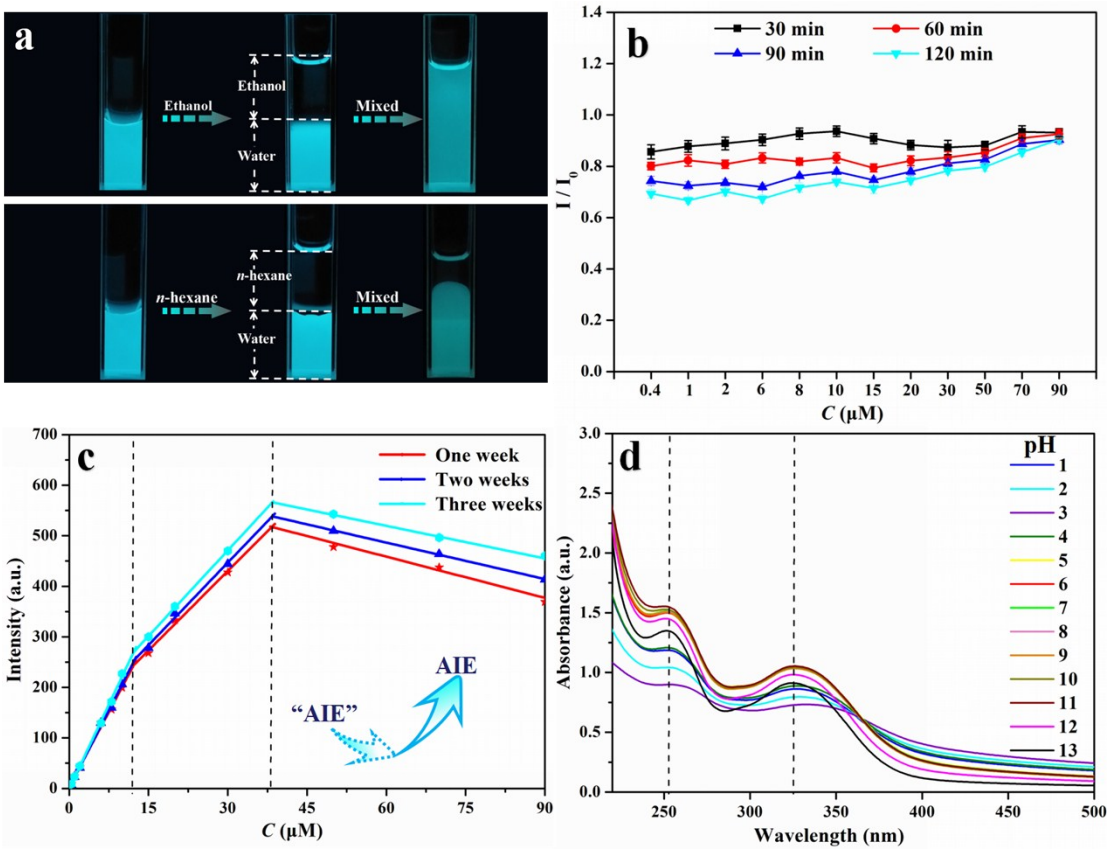

Figure S9. (a) Photographs of N_{16}-TPE-N_{16} aqueous solution when they were mixed with ethanol and *n*-hexane under the 365 nm UV irradiation. (b) Photostability of N_{16}-TPE-N_{16} upon continuous UV excitation at different concentrations. I_0 is the initial fluorescence intensity at 480 nm and I is the fluorescence intensity of the samples after UV irradiation. (c) Time-dependent evolution of the fluorescence intensity of N_{16}-TPE-N_{16} at different concentrations. (d) Absorption spectra of N_{16}-TPE-N_{16} at different pH values.

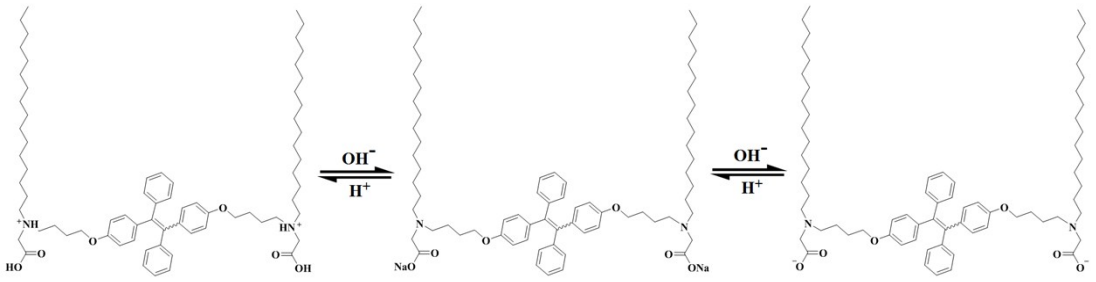

Figure S10. Chemical structural transformation of N_{16}-TPE-N_{16} at different H^+ concentrations.

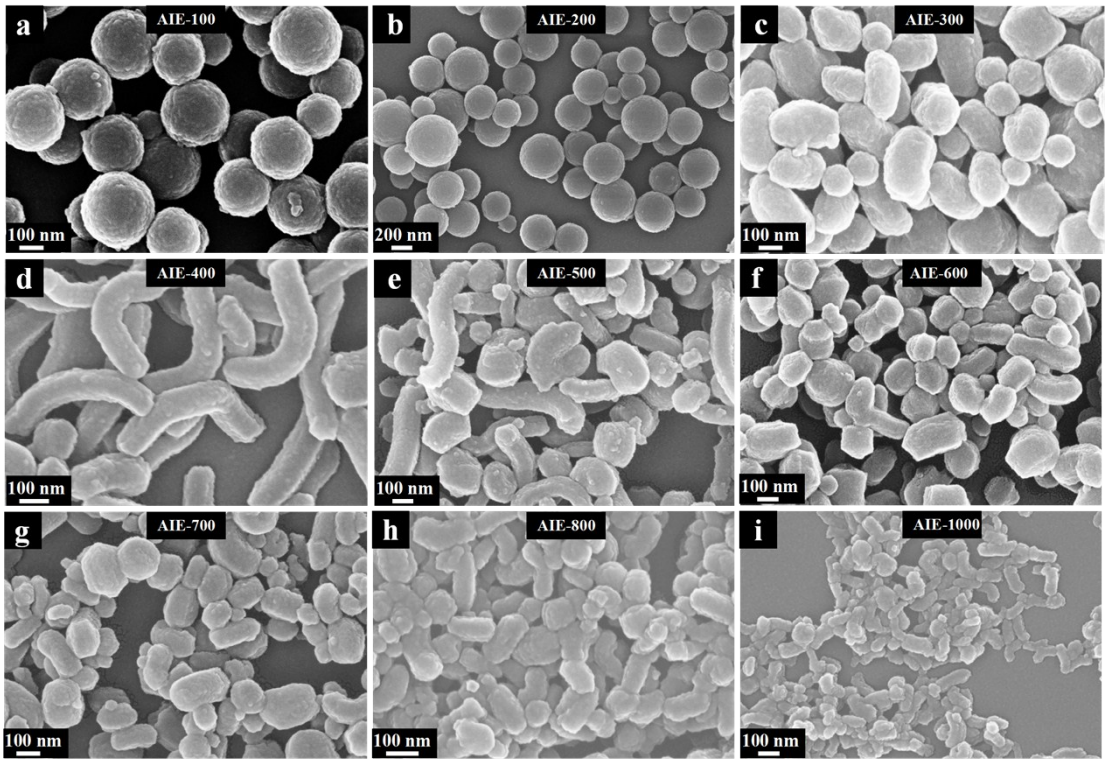

Figure S11. SEM images of AIE-SNs obtained under different concentrations of N_{16}-TPE-N_{16}: (a) 100, (b) 200, (c) 300, (d) 400, (e) 500, (f) 600, (g) 700, (h) 800, (i) 1000 μM.

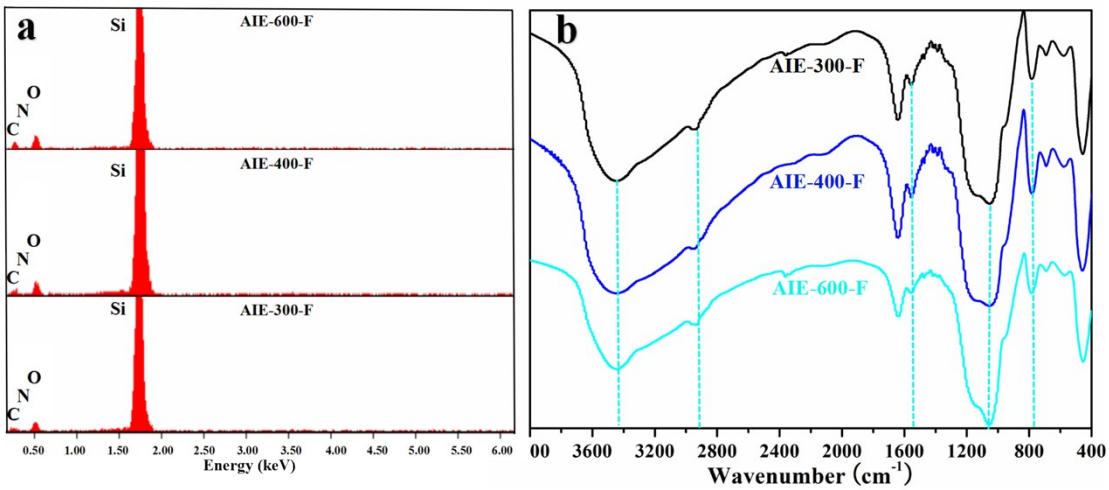

Figure S12. EDX patterns (a) and IR spectra (b) of AIE-300-F, AIE-400-F and AIE-600-F.

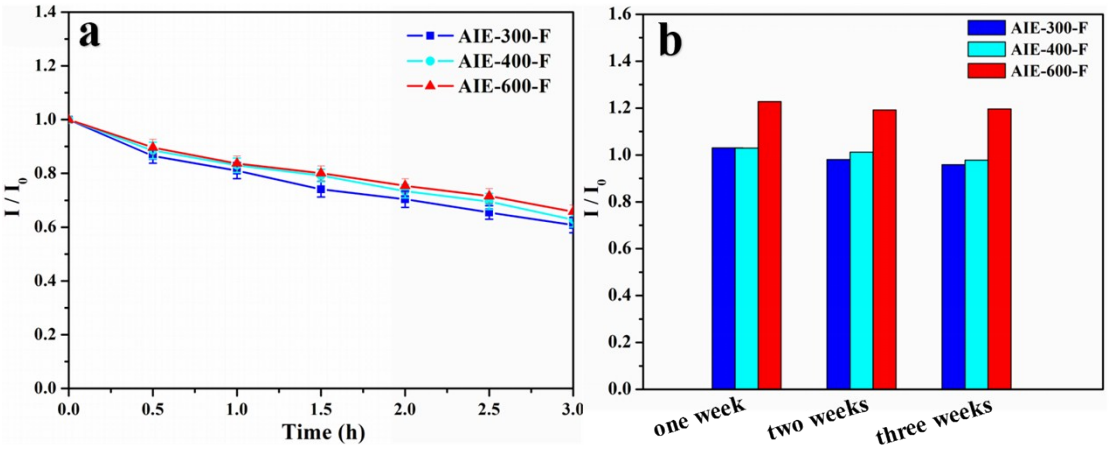

Figure S13. Photostability of AIE-300-F, AIE-400-F and AIE-600-F upon continuous UV excitation (a) and time-dependent evolution of the fluorescence intensity at different times (b). I_0 is the initial fluorescence intensity at 416 nm and I is the seasonable fluorescence intensity of the samples.

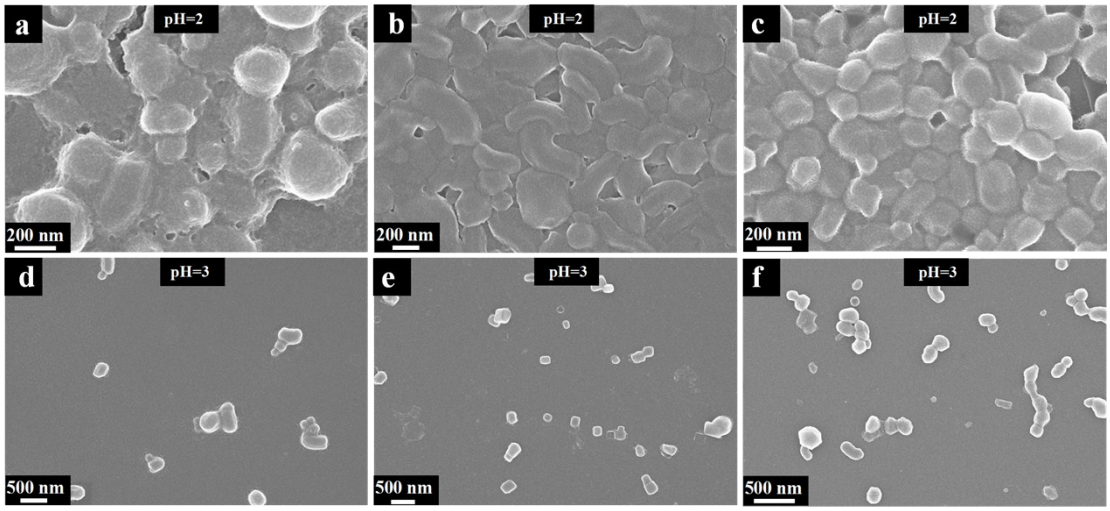

Figure S14. SEM images of AIE-300-F (a, d), AIE-400-F (b, e) and AIE-600-F (c, f) at pH = 2 and 3, respectively.

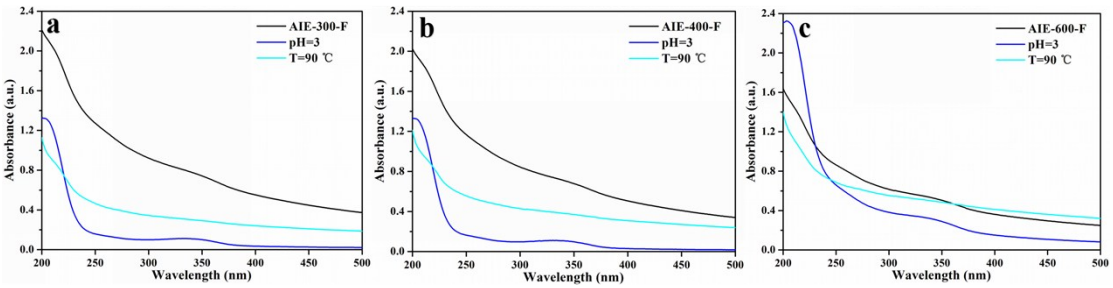

Figure S15. Absorption spectra of AIE-300-F (a), AIE-400-F (b) and AIE-600-F (c) at different states.

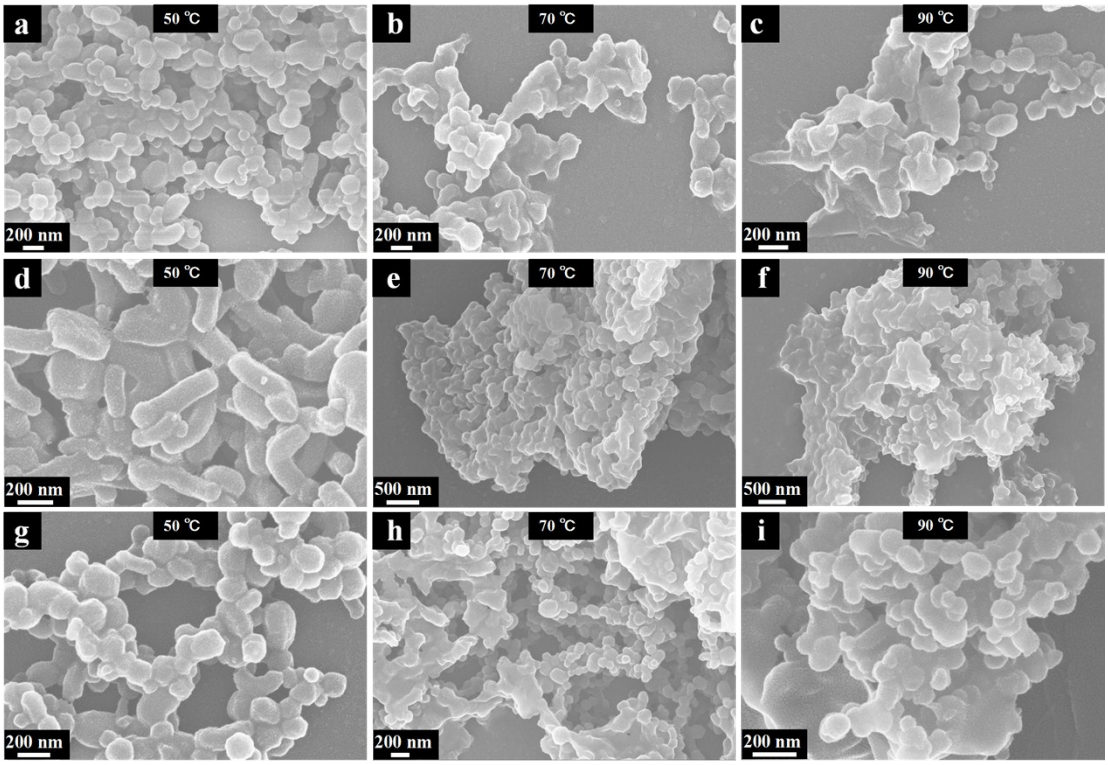

Figure S16. SEM images of AIE-300-F (a, b, c), AIE-400-F (d, e, f) and AIE-600-F (g, h, i) treated with different temperatures.

Table S1. The zeta-potential (ζ-potential) results of the SiO_2-NH_2, SiO_2-NH_2-F, AIE-300-F, AIE-400-F, AIE-600-F and CTAB-SNs.

Samples	ζ (mv)
SiO_2-NH_2	-1.55
SiO_2-NH_2-F	1.02
AIE-300-F	-3.11
AIE-400-F	-3.58
AIE-600-F	-4.39
CTAB-SNs	-46.5

Table S2. The elemental content (C, H, O, N) of as-prepared SiO_2-NH_2, SiO_2-NH_2-F, AIE-300-F, AIE-400-F and AIE-600-F by elemental analysis and EDX.

Samples	Elemental content (wt. %)			
	C	H	O	**N**
SiO_2-NH_2	10.93	4.477	27.91	**4.019**
SiO_2-NH_2-F	15.56	5.326	14.79	**5.229**
AIE-300-F	15.89	5.370	18.18	**5.294**
AIE-400-F	15.94	5.089	16.33	**5.027**
AIE-600-F	17.70	5.304	20.53	**4.962**

Table S3. A summary of experimental data and processing parameters.

Samples	Volume ratio of TEOS/APS	C^a (μM)	Morphology
SiO_2-NH_2	1:1	0	nanospheres
SiO_2-NH_2-F	1:1	0	nanospheres
SiO_2-NH_2-F-0	1:1	0	large aggregates
SiO_2-NH_2-F-3	3:1	0	rough nanospheres
SiO_2-NH_2-F-5	5:1	0	bone-like nanorods
SiO_2-NH_2-F-7	7:1	0	small nanorods
SiO_2-NH_2-F-9	9:1	0	small nanorods
CTAB-SNs	/	0	small nanorods
AIE-100-F	1:1	100	nanospheres
AIE-200-F	1:1	200	nanospheres
AIE-300-F	1:1	300	short nanorods
AIE-400-F	1:1	400	long nanorods
AIE-500-F	1:1	500	long and short nanorods
AIE-600-F	1:1	600	short nanorods
AIE-700-F	1:1	700	short nanorods
AIE-800-F	1:1	800	disordered short nanorods
AIE-1000-F	1:1	1000	irregular nanorods

[a] The initial concentration of N_{16}-TPE-N_{16} in the reaction system.

Table S4. The sensitivity of SiO_2-NH_2-F, AIE-300-F, AIE-400-F and AIE-600-F to pH changes calculated from the fluorescence intensity, especially for pH = 1 and 3.

Samples	I / I_0		$(I - I_0) / I_0 \times 100\%$	
	pH = 1	pH = 3	pH = 1	pH = 3
SiO_2-NH_2-F	0.99	0.52	-1.41	-92.38
AIE-300-F	1.04	0.55	**3.75**	-82.12
AIE-400-F	1.05	0.56	**4.48**	-77.69
AIE-600-F	1.03	0.68	**2.91**	-46.54

[a] I is the final fluorescence intensity at 416 nm after overnight and I_0 is the initial fluorescence intensity at 416 nm dispersed in water with different pH values.